nature medicine

The intracellular Ca^{2+} channel MCOLN1 is required for sarcolemma repair to prevent muscular dystrophy

Xiping Cheng[1], Xiaoli Zhang[1], Qiong Gao[1], Mohammad Ali Samie[1], Marlene Azar[1], Wai Lok Tsang[1], Libing Dong[1], Nirakar Sahoo[1], Xinran Li[1], Yue Zhuo[1], Abigail G Garrity[1,2], Xiang Wang[1], Marc Ferrer[3], James Dowling[4–8], Li Xu[9], Renzhi Han[9] & Haoxing Xu[1,2]

The integrity of the plasma membrane is maintained through an active repair process, especially in skeletal and cardiac muscle cells, in which contraction-induced mechanical damage frequently occurs *in vivo*[1,2]. Muscular dystrophies (MDs) are a group of muscle diseases characterized by skeletal muscle wasting and weakness[3,4]. An important cause of these group of diseases is defective repair of sarcolemmal injuries, which normally requires Ca^{2+} sensor proteins[5–8] and Ca^{2+}-dependent delivery of intracellular vesicles to the sites of injury[8,9]. MCOLN1 (also known as TRPML1, ML1) is an endosomal and lysosomal Ca^{2+} channel whose human mutations cause mucolipidosis IV (ML4), a neurodegenerative disease with motor disabilities[10,11]. Here we report that ML1-null mice develop a primary, early-onset MD independent of neural degeneration. Although the dystrophin-glycoprotein complex and the known membrane repair proteins are expressed normally, membrane resealing was defective in ML1-null muscle fibers and also upon acute and pharmacological inhibition of ML1 channel activity or vesicular Ca^{2+} release. Injury facilitated the trafficking and exocytosis of vesicles by upmodulating ML1 channel activity. In the dystrophic *mdx* mouse model, overexpression of ML1 decreased muscle pathology. Collectively, our data have identified an intracellular Ca^{2+} channel that regulates membrane repair in skeletal muscle via Ca^{2+}-dependent vesicle exocytosis.

We used PCR genotyping to confirm in our targeted mouse strain the presence of a genetic deletion of *Mcoln1* (referred to as ML1 KO)[11] (**Supplementary Fig. 1a**; see **Supplementary Data Set**). Using reverse transcription PCR (RT-PCR), we detected no full-length ML1 transcript in skeletal muscle and cultured myoblasts isolated from ML1 KO mice (**Fig. 1a**). Consistent with these results, patch-clamping of the endolysosomal membranes[12] showed that ML1-like currents (I_{ML1}) were activated in whole endolysosomes by ML-SA1, a membrane-permeable ML1-specific synthetic agonist[13], in wild-type (WT) but not ML1 KO primary cultured myoblasts (**Fig. 1b**). I_{ML1} was potently inhibited by ML-SI compounds (**Fig. 1b**), which are membrane-permeable ML-specific synthetic inhibitors[14].

At 1 month of age, ML1 KO mice are grossly healthy and do not show any obvious neurodegeneration[11]. However, when they are challenged with a 15° downhill treadmill test at the speed of 20 m/min, ML1 KO mice show a pronounced defect in their motor functions and a greatly reduced ability to remain on the treadmill (**Fig. 1c**). Histological analysis of various tissues involved in the movement impairment revealed, unexpectedly, that the skeletal muscles of ML1 KO mice had clear signs of dystrophy, even at 1 month of age (**Fig. 1d**,**e**). Indeed, by this early age, we detected individual necrotic and centrally nucleated fibers in ML1 KO skeletal muscle (**Fig. 1d**,**e**). In contrast, there was no obvious dystrophy in WT skeletal muscle at any age examined (**Fig. 1e**,**f**).

By 3 months of age, we commonly found central nucleation, fibrosis (fibrous scar tissue and fat replacement) and immune cell infiltration (**Fig. 1d**,**e** and **Supplementary Fig. 1**) in the skeletal muscles of ML1 KO mice. As observed in most animal models of MD[15], the distribution of the dystrophic area in skeletal muscle was heterogeneous. For example, for the gastrocnemius muscle, the dystrophic area was mainly concentrated on the periphery of the muscle and the central region remained largely intact (**Fig. 1d**). A characteristic of MD is muscle regeneration triggered by degeneration, forming a cycle of degeneration and regeneration[4,9]. Hence, centrally nucleated muscle fibers and smaller-sized fibers are frequently observed, reflecting muscles undergoing active regeneration[4,9]. Consistent with this finding, ML1 KO fibers were relatively small, with a high degree of central nucleation (**Fig. 1d**,**g**,**h**).

ML1 KO mice exhibited progressive MD, with severity increasing with age (**Fig. 1e–g**). Muscle-specific heterogeneity is common in patients with MD, potentially resulting from the variability in use-dependent physical activity of different muscles[3,4]. In 1-month-old

[1]Department of Molecular, Cellular, and Developmental Biology, University of Michigan, Ann Arbor, Michigan, USA. [2]Neuroscience Graduate Program, University of Michigan, Ann Arbor, Michigan, USA. [3]National Center for Advancing Translational Science, National Institutes of Health, Maryland, USA. [4]Department of Pediatrics, University of Michigan Medical Center, Ann Arbor, Michigan, USA. [5]Division of Neurology, Hospital for Sick Children, Toronto, Ontario, Canada. [6]Program of Genetic and Genome Biology, Hospital for Sick Children, Toronto, Ontario, Canada. [7]Department of Pediatrics, University of Toronto, Toronto, Ontario, Canada. [8]Department of Molecular Genetics, University of Toronto, Toronto, Ontario, Canada. [9]Department of Cell and Molecular Physiology, Loyola University Chicago Health Sciences Division, Chicago, Illinois, USA. Correspondence should be addressed to H.X. (haoxingx@umich.edu) or X.C. (xpcheng@umich.edu).

Received 5 March; accepted 19 May; published online 14 September 2014; doi:10.1038/nm.3611

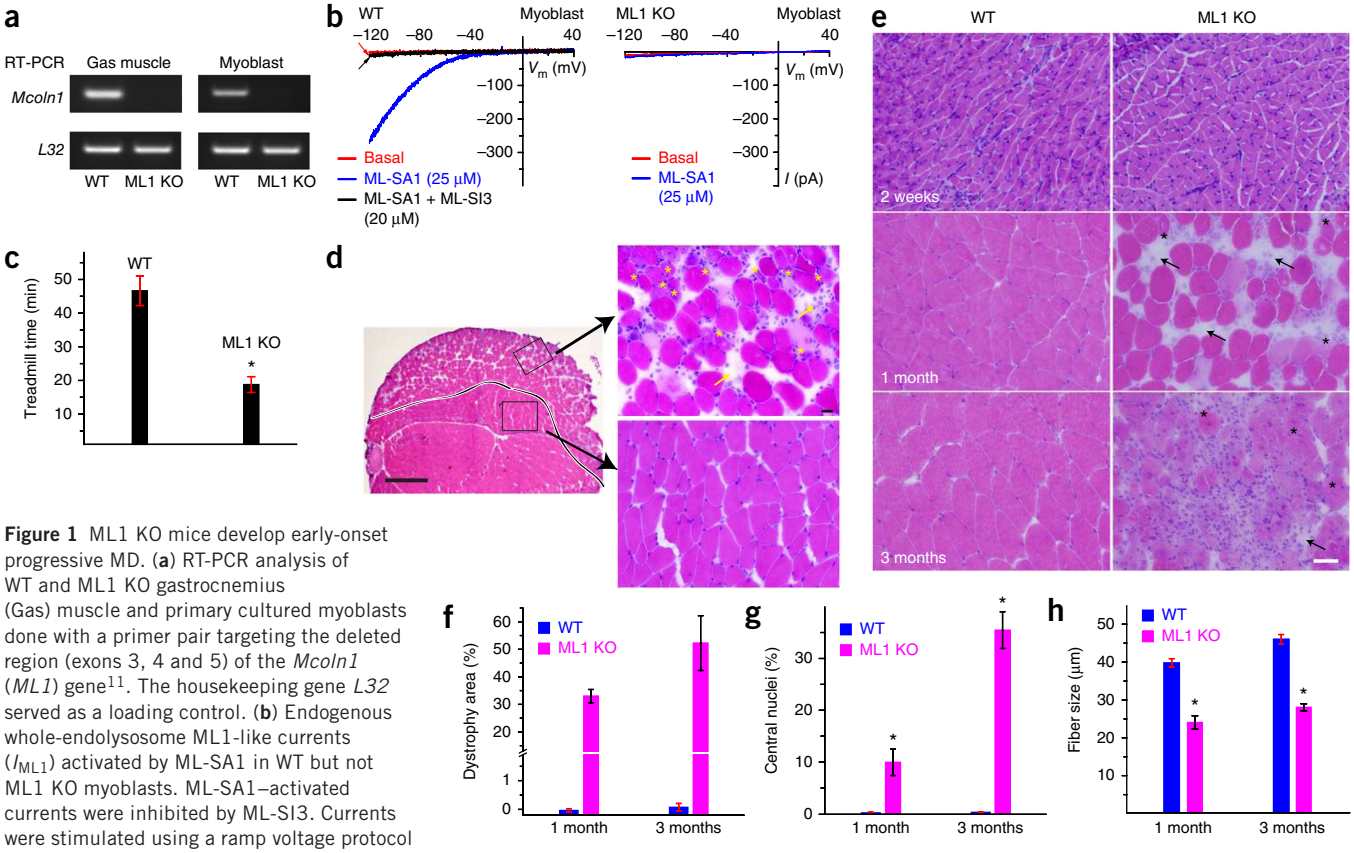

Figure 1 ML1 KO mice develop early-onset progressive MD. (**a**) RT-PCR analysis of WT and ML1 KO gastrocnemius (Gas) muscle and primary cultured myoblasts done with a primer pair targeting the deleted region (exons 3, 4 and 5) of the *Mcoln1* (*ML1*) gene[11]. The housekeeping gene *L32* served as a loading control. (**b**) Endogenous whole-endolysosome ML1-like currents (I_{ML1}) activated by ML-SA1 in WT but not ML1 KO myoblasts. ML-SA1–activated currents were inhibited by ML-SI3. Currents were stimulated using a ramp voltage protocol from −120 to +40 mV. (**c**) Treadmill persistence time of one-month-old ML1 KO mice and WT controls ($n = 5$ animals for each condition). $^*P < 0.05$. (**d**) H&E staining of a gastrocnemius muscle section from a 1-month-old ML1 KO mouse. Scale bar, 400 μm. The black line indicates the boundary between the dystrophic region at the periphery and the normal region in the center. The images on the right (representative of 16 sections total from 4 mice) provide a close-up view of the boxed areas (left) and show the centrally nucleated fibers (asterisks) and fibrosis (arrows). Scale bar, 20 μm. (**e**) H&E staining of gastrocnemius muscle sections from ML1 KO and WT mice at 2 weeks, 1 month and 3 months of age. Scale bar, 20 μm. Images are representative of 20 sections total from 5 pairs of mice. (**f**) The percentage of the dystrophic area in ML1 KO and WT muscle. (**g**) The percentage of centrally nucleated fibers in ML1 KO and WT muscle. (**h**) The diameters of muscle fibers in ML1 KO and WT mice. For panels **f**–**h**, $n = 3$ animals for each condition. Data are presented as the mean ± s.e.m. $^*P < 0.05$.

ML1 KO mice, only about half of the skeletal muscles, including the triceps, quadriceps, hamstring and gastrocnemius muscles, manifested dystrophy (**Supplementary Fig. 1c**). In contrast, the diaphragm, iliopsoas, gluteus, soleus and tibialis anterior muscles appeared normal (**Supplementary Fig. 1c**). However, by 3 months of age, more skeletal muscles developed dystrophy (**Supplementary Fig. 1d**). Both type 1 slow-twitch and type 2 fast-twitch muscle fibers were dystrophic (**Supplementary Fig. 2a**). However, cardiac and smooth muscles in 3-month-old ML1 KO mice did not show obvious pathology (**Supplementary Fig. 2b**). These results suggest that ML1 KO mice exhibited early-onset, progressive and extensive MD.

Evans blue (EB) dye is a reliable *in vivo* marker of myofiber damage[16]. A small but significant percentage of ML1 KO gastrocnemius myofibers were EB positive at rest (**Fig. 2a**,**b**). After a 15° downhill treadmill exercise, the percentage of EB-positive cells in the ML1 KO gastrocnemius muscle increased from 2% to 12% (**Fig. 2a**,**b**). In comparison, the percentage of EB-positive cells in WT littermates never exceeded 1%, even after treadmill exercise (**Fig. 2a**,**b**).

Another measure of myofiber damage is the leakage of muscle proteins into the serum[3,4]. Consistent with the EB analysis, the serum creatine kinase (CK) levels of ML1 KO mice were two- to three-fold higher than those of their WT littermates (**Fig. 2c**). Treadmill exercise increased serum CK levels further (**Fig. 2c**). These results suggest that an increase in muscle membrane damage underlies MD in ML1 KO mice.

Although muscle pathology and elevated CK levels were initially reported in some ML4 patients[17,18], ML4 has generally been considered a disease of neural degeneration[10,11], which could explain the motor defects of ML4 patients and ML1 KO mice. Consistent with previous reports[11,19], ML1 KO mice did exhibit neuronal cell death, but only at ages >5 months (**Supplementary Fig. 2c**). At younger ages (1–3 months), motor neurons in the spinal cord did not show any obvious sign of neural degeneration (**Supplementary Fig. 2d**). Likewise, sciatic nerve myelination was normal in ML1 KO mice at 1 month of age (**Fig. 2d**). Furthermore, in conditions mimicking neural degeneration, such as sciatic nerve axotomy, we did not observe a dystrophic phenotype (**Fig. 2e**). Instead, axotomy resulted in muscle atrophy, which manifested as a homogeneous decrease in fiber size (**Fig. 2e**). In addition, gastrocnemius muscle from the mouse model of Fabry's disease[20] showed denervation-like effects on the fiber size but not MD-like necrosis or central nucleation (**Fig. 2f**). In 1-month-old ML1 KO mice, we saw only minimal evidence of lysosomal storage disease (LSD) in the dystrophic muscles (**Supplementary Fig. 2e**). These results suggest that muscle dystrophy in the ML1 KO mice is unlikely to be a secondary effect of neural degeneration or a lysosome storage defect.

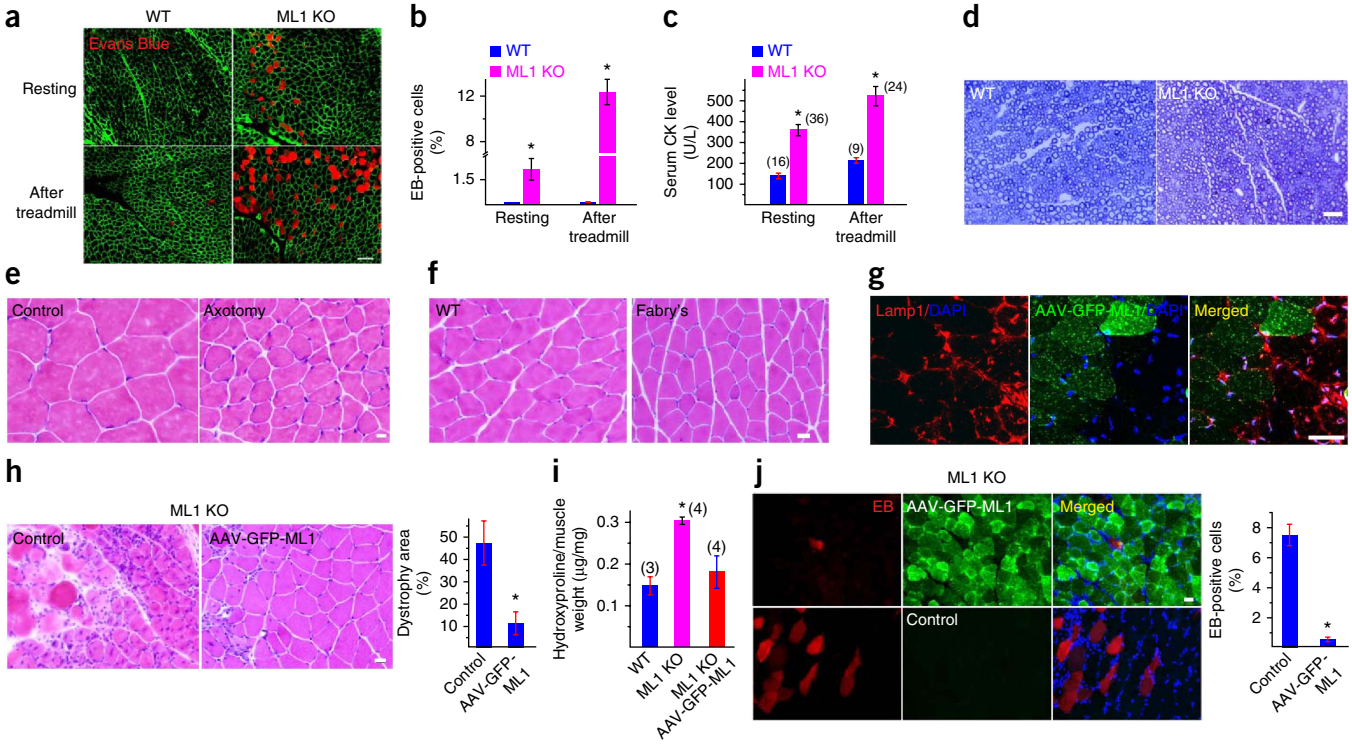

Figure 2 MD and muscle membrane damage of ML1 KO mice are not caused by neural degeneration and can be rescued by muscle expression of ML1. (**a**) EB dye staining (red) in WT and ML1 KO gastrocnemius muscles either at rest or after a 30-min treadmill test at the speed of 12 m/min. Immunostaining of α-dystroglycan (α-DG) (green) was used to label the sarcolemma. Scale bar, 40 μm. Images are representative of overall 26 sections from 6 pairs of mice. (**b**) The percentage of EB-positive muscle fibers in WT and ML1 KO mice ($n = 3$ animals for each condition). $^*P < 0.05$. (**c**) Serum CK levels in WT and ML1 KO mice, either before or after treadmill exercise. The number of animals for each condition is indicated in the parentheses. $^*P < 0.05$. (**d**) Lack of obvious myelination defects in the sciatic nerve of 1-month-old ML1 KO mice. Scale bar, 10 μm. Images are representative of 8 sections total from 2 pairs of mice. (**e**) Sciatic axotomy induced atrophy of WT gastrocnemius muscle. Scale bar, 10 μm. Images are representative of 12 sections total from 3 mice. (**f**) Atrophic gastrocnemius muscle of 4-month-old Fabry's mice. Scale bar, 20 μm. Images are representative of 8 sections total from 2 pairs of mice. (**g**) AAV-GFP-ML1 infection reduces Lamp1 elevation in ML1 KO muscle cells compared with neighboring uninfected controls. Scale bar, 40 μm. Images are representative of 16 sections total from 4 mice. (**h**) Left, H&E staining to reveal the degree of necrosis and fibrosis in muscle from ML1 KO mice with and without infection with AAV-GFP-ML1. Right, the percentage of the dystrophic area in these muscles ($n = 4$ animals for each condition). Scale bar, 10 μm. Images are representative of 16 sections total from 4 mice. (**i**) Collagen content as measured by hydroxyproline content in muscle from 3-month-old WT mice and ML1 KO mice before or after AAV-GFP-ML1 infection. (**j**) Left, EB dye uptake (red) in muscle from ML1 KO mice with or without AAV-GFP-ML1 infection (green). Scale bar, 10 μm. Images are representative of 12 sections total from 3 mice. Right, the percentage of the EB positive cell in muscle from ML1 KO mice with or without AAV-GFP-ML1 infection ($n = 3$ animals for each condition). Data are presented as the mean ± s.e.m. For panels **h**-**j**, $^*P < 0.05$.

To investigate directly the dystrophic mechanisms caused by ML1 deficiency, we performed a rescue experiment involving intramuscular injection of an adeno-associated virus (AAV) carrying the GFP-ML1 transgene (AAV-GFP-ML1), which typically infected most (>85%) of the muscle fibers. As observed in many lysosomal storage disorders (LSDs), ML1 KO muscle showed a compensatory increase in the key lysosomal protein Lamp1 (ref. 13), as indicated by Lamp1 immunofluorescence staining and western blot analysis (**Supplementary Fig. 3a**,**b**). However, when compared with the uninfected adjacent and contralateral muscle fibers, ML1 KO gastrocnemius muscle infected with AAV-GFP-ML1 (localized in Lamp1-positive compartments; **Supplementary Fig. 3c**,**d**) showed a strong AAV infection–mediated decrease of elevated Lamp1 expression (**Fig. 2g** and **Supplementary Fig. 3e**). AAV-ML1-GFP infection reduced the dystrophic area (**Fig. 2h**) and collagen content (**Fig. 2i**) of the muscle as well as the percentage of EB-positive muscle fibers (**Fig. 2j**). Hence, expression of ML1 in muscle was sufficient to rescue the MD of ML1 KO mice, suggesting a cell-autonomous mechanism as the underlying cause of MD in these mice.

Mechanical stress can cause myofiber necrosis by two separate mechanisms. First, the sarcolemma of a muscle fiber could be more susceptible to damage, as seen in dystrophin (a core component of the dystrophin-glycoprotein complex (DGC)) mutant (*mdx*) mice[4,21]. Second, a muscle fiber could have a defect in sarcolemma repair, as seen in dysferlin or MG53 knockout mice[5,9,22]. Most human MD mutations are linked to defects in the components of the DGC[4]. However, we saw no obvious decrease in expression of any of the core or accessory components of the DGC that we examined, which included dystrophin, β-dystroglycan (β-DG), integrin β1 and laminin (**Fig. 3a**,**b**). Furthermore, the expression of dysferlin, caveolin 3 and MG53, three proteins known to be involved in sarcolemma repair and human MD[4,5,23], also showed no decrease in ML1 KO muscle (**Fig. 3a**,**b**).

To create plasma membrane disruptions and to evaluate the resealing efficiency, we irradiated single myofibers isolated from the flexor digitorum brevis (FDB) muscle of WT and ML1 KO mice using a two-photon laser[5,9]. FM1-43, a membrane-impermeable fluorescent dye that preferentially adheres to lipids, is commonly used to detect membrane disruptions[5]. We observed rapid entry and accumulation

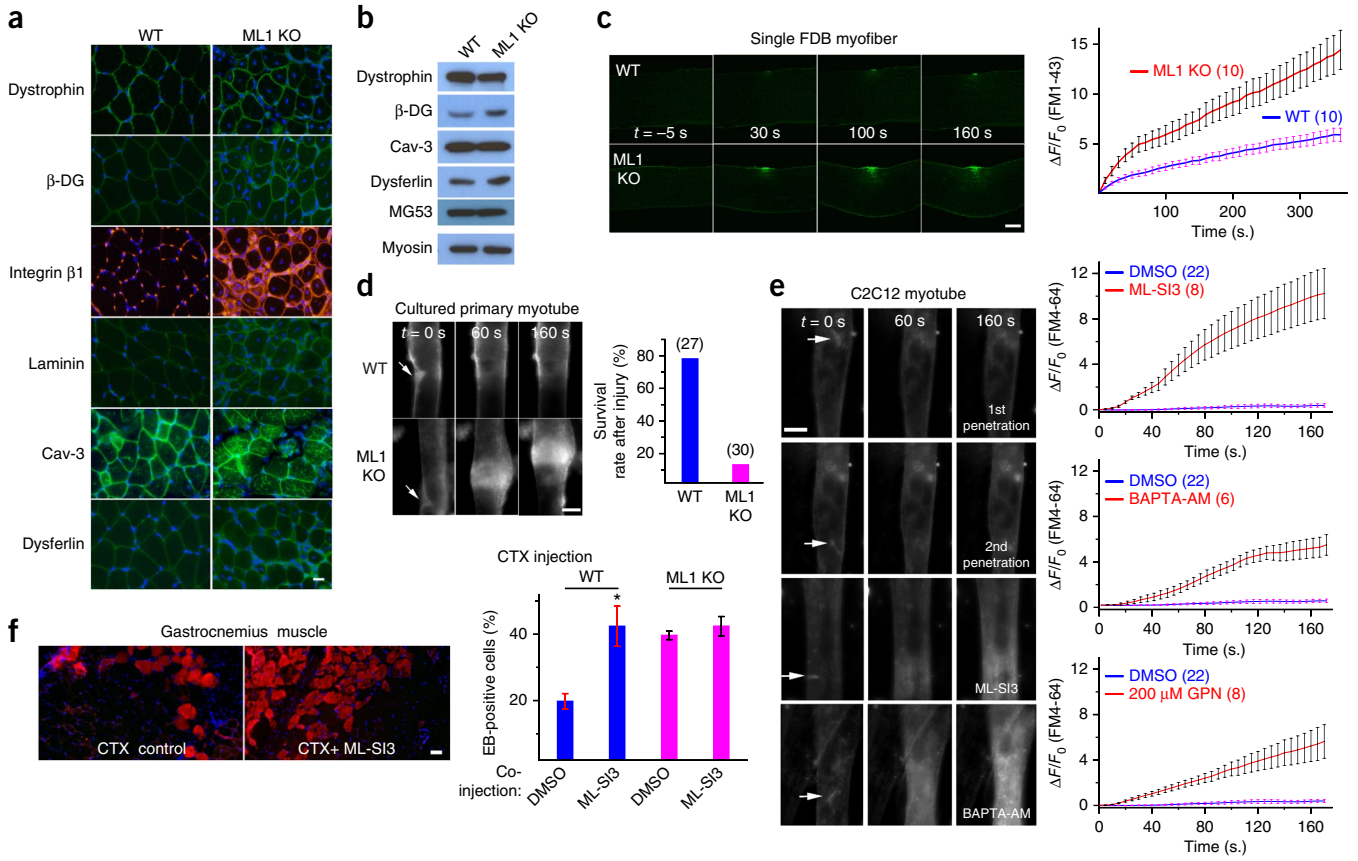

Figure 3 Defective membrane repair capacity in ML1 KO muscle. (**a**) Immunofluorescence of dystrophin, β-dystroglycan (β-DG), integrin β1, laminin, caveolin-3 (Cav-3) and dysferlin in gastrocnemius muscle from WT and ML1 KO mice. Scale bar, 10 μm. Images are representative of overall 24-30 sections from 4 or 5 pairs of mice. (**b**) Western blot analysis of the DGC components, Cav-3, dysferlin and MG53 in WT and ML1 KO mice. Myosin served as a loading control. (**c**) A membrane repair assay performed on single FDB muscle fibers isolated from WT and ML1 KO mice. Membrane damage was induced with a two-photon laser at $t = 0$ s. Scale bar, 10 μm. Right, time-dependent changes (ΔF) in FM1-43 fluorescence intensity normalized to the basal fluorescence (F_0) for WT (blue) and ML1 KO (red) fibers. (**d**) Representative images of *in vitro*–differentiated myotubes in response to mechanical damage elicited by a microelectrode (arrows). Right, percentage of myotubes 'surviving' in response to microelectrode penetration. The experiments were performed in the presence of extracellular Ca^{2+}, and defective membrane resealing led to excessive Ca^{2+} influx, which triggered prolonged muscle contraction. The surviving cells are those without prolonged contraction. Scale bar, 50 μm. (**e**) Responses of C2C12-derived myotubes to microelectrode penetration in Tyrode's solution (2 mM Ca^{2+}) in the presence of DMSO (0.1%; first and second penetration), ML-SI3 (20 μM), BAPTA-AM (20 μM) and GPN (200 μM). Right, time course of FM4-64 accumulation ($\Delta F/F_0$) at injury sites following microelectrode penetration. Scale bar, 50 μm. The same set of DMSO control data was compared with all groups of drug treatment data. (**f**) The effect of ML-SI3, a ML-specific synthetic inhibitor, on EB dye uptake in WT gastrocnemius muscles injected with the cardiotoxin VII4 (CTX), a cytolytic toxin that disrupts cell membrane in living animals[24]. Right, effect of intramuscular co-injection of ML-SI3 with CTX on EB dye uptake in muscle from WT and ML1 KO mice ($n = 3$ animals for each condition). Images are representative of overall 15 sections from 3 experiments. Scale bar, 10 μm. Data are presented as the mean ± s.e.m. $^*P < 0.05$.

of FM1-43 dye within seconds after laser irradiation (**Fig. 3c** and **Supplementary Fig. 4a**). However, in WT muscle fibers, dye entry ceased shortly (1–2 min) after irradiation, suggesting successful membrane resealing (**Fig. 3c**). In contrast, upon identical laser irritation of fibers from ML1 KO mice, uptake of the FM1-43 dye continued at the injury sites for several minutes (**Fig. 3c**), suggesting failed membrane resealing. Removal of extracellular Ca^{2+} caused rapid accumulation of FM1-43 dye at the injury sites, which was indistinguishable for myofibers from WT and ML1 KO mice (**Supplementary Fig. 4b**). We also observed defective membrane resealing in myotubes from ML1 KO mice that were exposed to mechanical damage elicited by microelectrode penetration into the sarcolemmal membrane (**Fig. 3d**). Unlike most myotubes from WT mice, most (>80%) of those from ML1 KO mice could not 'survive' the prolonged contractions caused by continuous Ca^{2+} entry.

Next, we performed pharmacological experiments on myotubes derived from the C2C12 mouse cell line using the microelectrode penetration assay[24]. We did not see substantial uptake of FM4-64 dye (a red-colored analog of the FM1-43 dye) at injury sites, even with repeated penetrations (**Fig. 3e**). In contrast, removal of extracellular Ca^{2+} substantially increased the entry of FM dyes (**Supplementary Fig. 4c**), suggesting that the influx of extracellular Ca^{2+} is essential for repair[8]. In the presence of BAPTA-AM, used to chelate intracellular Ca^{2+}, or glycyl-L-phenylalanine 2-naphthylamide (GPN), a lysosome-targeted cathepsin C substrate, to specifically deplete the lysosomal Ca^{2+} store[13], we observed substantial dye entry even under normal extracellular Ca^{2+} concentrations (2 mM; **Fig. 3e**). These results suggest that lysosomal Ca^{2+} also has a role in membrane resealing.

To monitor the Ca^{2+} levels at injury sites, we transfected myoblasts from WT and ML1 KO mice and C2C12 cells with Lamp1-GCaMP3,

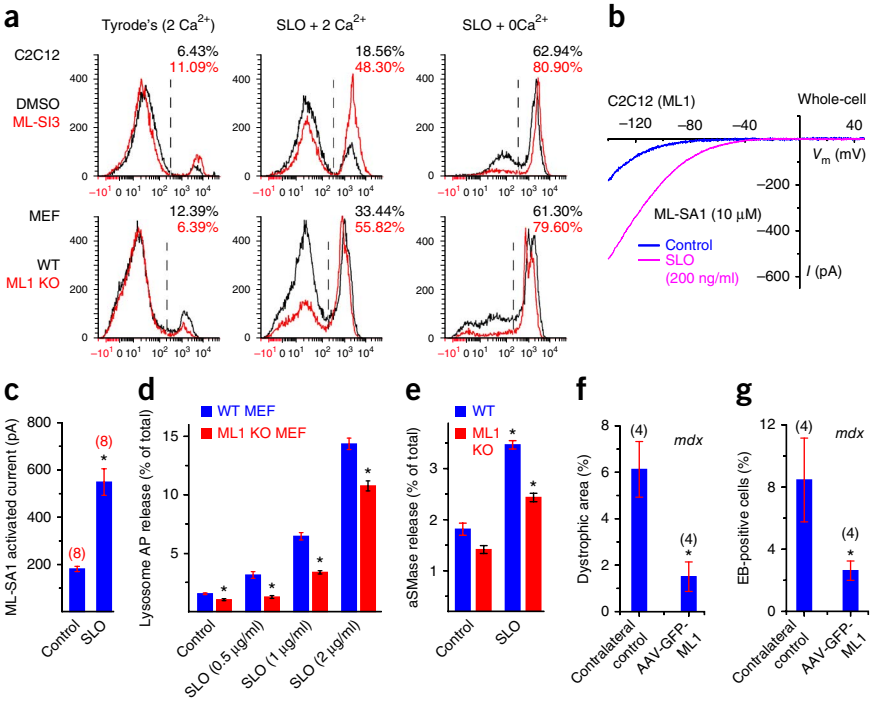

Figure 4 ML1 has an essential role in lysosomal exocytosis, membrane repair and protection of muscle damage *in vivo*. (**a**) C2C12 and MEF cells were treated with the pore-forming toxin SLO (2–5 μg/ml) and stained with PI, a marker for membrane damage. Fluorescence-activated cell sorting (FACS) quantification of PI staining was performed in cells with or without SLO or external Ca^{2+} (2 mM). Tyrode's, standard extracellular solution (2 mM Ca^{2+}). Images are representative of overall 4 experiments. (**b**,**c**) Whole-cell I_{ML1} in C2C12 cells transfected with GFP-ML1 with or without SLO treatment were recorded. $^*P < 0.05$. (**d**) SLO (0.5 μg/ml, 1 μg/ml and 2 μg/ml for 15 min) treatment on the release of lysosomal acid phosphatase (AP; determined using an AP activity colorimetric assay kit) into the culture medium in WT and ML1 KO MEFs. The data are presented as the percentage of the activity of the released versus total cell-associated enzymes. (**e**) SLO (0.5 μg/mL for 15 min) treatment on the release of lysosomal acid SMase (aSMase; determined using an aSMase activity assay kit) in WT and ML1 KO MEFs. (**f**,**g**) Dystrophic area and EB uptake in gastrocnemius muscle from *mdx* mice after AAV-GFP-ML1 infection versus contralateral uninfected control tissue. Data are presented as the mean ± s.e.m. For panels **d**–**g**, $^*P < 0.05$.

a lysosome-targeted genetically encoded Ca^{2+} indicator[13]. We observed transient Ca^{2+} increases at injury sites in the presence or absence of external Ca^{2+} (**Supplementary Fig. 4d**–**g**). However, release of intracellular Ca^{2+} was less in myoblasts from ML1 KO mice or in the presence of ML-SI compounds[14] (**Supplementary Fig. 4f**,**g**), suggesting a contribution to Ca^{2+} release from lysosomes during membrane damage or the early stage of membrane repair. In the presence of external Ca^{2+}, we observed a prolonged Ca^{2+} influx in myoblasts from ML1 KO mice or ML-SI3-treated C2C12 myoblasts (**Supplementary Fig. 4d**,**e**). Hence, ML1 has a dual role in promoting the initial phase of Ca^{2+} increase (within seconds) but inhibiting the prolonged phase of Ca^{2+} increase (lasting minutes).

To test whether ML1 has a direct role in membrane repair, we acutely inhibited ML1 channel function using ML-SIs. Notably, in experiments performed by researchers who were blind to experimental conditions, substantial FM4-64 dye uptake was seen in the presence of three structurally independent ML-SI compounds (**Fig. 3e** and **Supplementary Fig. 4c**). We also used ML1 inhibitors to test the role of ML1 in sarcolemma repair *in vivo*. Cardiotoxin VII4 (CTX) is a toxin that can induce membrane damage *in vivo* to cause EB dye accumulation in muscle cells[24]. EB-positive muscle cells were more numerous in CTX-treated muscle from ML1 KO mice than in muscle from CTX-treated WT control mice (**Supplementary Fig. 4h**). Notably, co-injection of ML-SI3 with CTX markedly increased the percentage of EB-positive muscles in CTX-treated WT mice, to the same level as in CTX-treated ML1 KO mice (**Fig. 3f** and **Supplementary Fig. 4h**).

Chemical injuries from streptolysin O (SLO) toxin is often used to induce membrane repair responses, and propidium iodide (PI) staining is a common readout for membrane damage and cell viability[25]. In non-muscle cells, including mouse embryonic fibroblasts (MEFs) and bone marrow–derived macrophages (BMMs), treatment with SLO resulted in more PI-positive cells from ML1 KO mice than from WT mice (**Fig. 4a** and **Supplementary Fig. 5**). In addition, ML-SI3 increased PI staining in WT, but not knockout cells (**Fig. 4a** and **Supplementary Fig. 5**). Conversely, ML1 overexpression decreased PI staining (**Supplementary Fig. 5**). These results suggest that ML1 may be a core component of the membrane repair machinery in both muscle and non-muscle cells.

Membrane resealing requires the fusion and exocytosis of intracellular vesicles at sarcolemma injury sites[8]. Upon SLO treatment, pHluorin total internal reflection fluorescence (TIRF) imaging[26] showed that ML1 and Vamp7 doubly-positive vesicles underwent exocytosis (**Supplementary Fig. 6a** and **Supplementary Video 1**). Exocytosis of ML1-resident vesicles may lead to the appearance of ML1 proteins at the plasma membrane. Hence, measurement of whole-cell ML1 currents may provide a readout for exocytosis[14]. Consistently, SLO treatment also increased whole-cell I_{ML1} by two-fold to three-fold in C2C12 cells (**Fig. 4b**,**c**). In contrast, ML-SI3–mediated inhibition of ML1, or knockout of ML1, substantially reduced SLO-induced lysosomal exocytosis as measured by Lamp1 surface staining[27] (**Supplementary Fig. 6b**,**c**) and release of lysosomal enzymes (acid phosphatase, AP, or acid sphingomyelinase, acid SMase[28]) (**Fig. 4d**,**e**) in muscle cells and MEFs. Collectively, these results suggest that ML1-mediated lysosomal exocytosis has an important role in membrane resealing.

Consistent with the possibility that overexpression of ML1 promotes membrane repair in *mdx* muscle[4,21], EB dye uptake and dystrophic area were both substantially less in AAV-GFP-ML1–infected muscle than in the contralateral noninjected control muscle of *mdx* mice(**Fig. 4f**,**g**).

ML1 KO mice exhibit a primary early-onset MD that is caused by defective membrane resealing. A similar but less dramatic dystrophic phenotype is observed in mice lacking MG53 or dysferlin, two proteins known to be involved in membrane repair[5,9]. By interacting with Ca^{2+} sensors in the vesicles, for example, dysferlin and Syt-VII[5,6], ML1 may mediate membrane repair by promoting vesicle exocytosis in both muscle and non-muscle cells (**Supplementary Fig. 7**). The initial rapid Ca^{2+} increase, in 10–20 s, is essential for triggering the resealing process. Depending on the nature of the damage and the size

of the wound, three different mechanisms may be used for membrane repair: membrane patching, endocytosis and shedding[8,28,29]. Previous studies have unequivocally established the roles of extracellular Ca^{2+} in all *in vitro* assays and models of membrane repair[5,27,29]. We show here that lysosomal Ca^{2+} is also essential for this process, even in the presence of extracellular Ca^{2+}, suggesting an involvement of more than one Ca^{2+} source. Consistent with this idea, multiple Ca^{2+} sensors are implicated in sarcolemma repair, including dysferlin, myoferlin, annexin, Syt-VII, Alix/ALG-2 and calcineurin[8,29].

Although lysosomes have long been implicated in membrane repair in non-muscle cells[27], their role in sarcolemma repair has remained unclear. Notably, expression of the housekeeping lysosomal protein Lamp1, which is compensatorily upregulated in many LSDs, is also elevated in dysferlin-null mice[30]. In addition, mice lacking Syt-VII, a lysosome-specific Ca^{2+} sensor, exhibit a MD-like phenotype[6]. Hence, the sarcolemma repair system may have a close relationship with the late endocytic pathway.

METHODS

Methods and any associated references are available in the online version of the paper.

Note: Any Supplementary Information and Source Data files are available in the online version of the paper.

ACKNOWLEDGMENTS

This work was supported by National Institutes of Health (NIH) grants (NS062792, MH096595 and AR060837 to H.X.; HL116546 and AR064241 to R.H.). We are grateful to S. Slaugenhaupt for the ML1 KO mice, L. Looger for the GCaMP3 construct, R. Edwards for the Vamp7-pHluorin construct, the Center for Live-Cell Imaging at the University of Michigan for the help on TIRF Imaging, and R. Hume and M. Akaaboune for comments on the manuscript. We appreciate the encouragement and helpful comments of other members of the Xu laboratory.

AUTHOR CONTRIBUTIONS

X.C. initiated the project; H.X., X.C., J.D. and R.H. designed the research; X.C., X.Z., Q.G., M.A.S., M.A., W.L.T., Y.Z. and L.D. performed the research; N.S., X.L., A.G.G., X.W., M.F. and L.X. contributed the new reagents; X.C., X.Z., Q.G., M.A.S., M.A., W.L.T., J.D., R.H. and H.X. analyzed the data; H.X. and X.C. wrote the paper with input from all the authors.

COMPETING FINANCIAL INTERESTS

The authors declare no competing financial interests.

1. Clarke, M.S., Khakee, R. & McNeil, P.L. Loss of cytoplasmic basic fibroblast growth factor from physiologically wounded myofibers of normal and dystrophic muscle. *J. Cell Sci.* **106**, 121–133 (1993).
2. McNeil, P.L. & Khakee, R. Disruptions of muscle fiber plasma membranes. Role in exercise-induced damage. *Am. J. Pathol.* **140**, 1097–1109 (1992).
3. Davies, K.E. & Nowak, K.J. Molecular mechanisms of muscular dystrophies: old and new players. *Nat. Rev. Mol. Cell Biol.* **7**, 762–773 (2006).
4. Rahimov, F. & Kunkel, L.M. The cell biology of disease: cellular and molecular mechanisms underlying muscular dystrophy. *J. Cell Biol.* **201**, 499–510 (2013).
5. Bansal, D. *et al.* Defective membrane repair in dysferlin-deficient muscular dystrophy. *Nature* **423**, 168–172 (2003).
6. Chakrabarti, S. *et al.* Impaired membrane resealing and autoimmune myositis in synaptotagmin VII-deficient mice. *J. Cell Biol.* **162**, 543–549 (2003).
7. Barresi, R. *et al.* LARGE can functionally bypass alpha-dystroglycan glycosylation defects in distinct congenital muscular dystrophies. *Nat. Med.* **10**, 696–703 (2004).
8. McNeil, P. Membrane repair redux: redox of MG53. *Nat. Cell Biol.* **11**, 7–9 (2009).
9. Cai, C. *et al.* MG53 nucleates assembly of cell membrane repair machinery. *Nat. Cell Biol.* **11**, 56–64 (2009).
10. Sun, M. *et al.* Mucolipidosis type IV is caused by mutations in a gene encoding a novel transient receptor potential channel. *Hum. Mol. Genet.* **9**, 2471–2478 (2000).
11. Venugopal, B. *et al.* Neurologic, gastric, and opthalmologic pathologies in a murine model of mucolipidosis type IV. *Am. J. Hum. Genet.* **81**, 1070–1083 (2007).
12. Dong, X.P. *et al.* The type IV mucolipidosis-associated protein TRPML1 is an endolysosomal iron release channel. *Nature* **455**, 992–996 (2008).
13. Shen, D. *et al.* Lipid storage disorders block lysosomal trafficking by inhibiting a TRP channel and lysosomal calcium release. *Nat. Commun.* **3**, 731 (2012).
14. Samie, M. *et al.* A TRP channel in the lysosome regulates large particle phagocytosis via focal exocytosis. *Dev. Cell* **26**, 511–524 (2013).
15. de Figueiredo, P. & Brown, W.J. A role for calmodulin in organelle membrane tubulation. *Mol. Biol. Cell* **6**, 871–887 (1995).
16. Straub, V., Rafael, J.A., Chamberlain, J.S. & Campbell, K.P. Animal models for muscular dystrophy show different patterns of sarcolemmal disruption. *J. Cell Biol.* **139**, 375–385 (1997).
17. Weitz, R. *et al.* Muscle involvement in mucolipidosis IV. *Brain Dev.* **12**, 524–528 (1990).
18. Zlotogora, J., Ben Ezra, D., Livni, N., Ashkenazi, A. & Cohen, T. A muscle disorder as presenting symptom in a child with mucolipidosis IV. *Neuropediatrics* **14**, 104–105 (1983).
19. Venugopal, B. *et al.* Chaperone-mediated autophagy is defective in mucolipidosis type IV. *J. Cell. Physiol.* **219**, 344–353 (2009).
20. Abe, A. *et al.* Reduction of globotriaosylceramide in Fabry disease mice by substrate deprivation. *J. Clin. Invest.* **105**, 1563–1571 (2000).
21. Campbell, K.P. Three muscular dystrophies: loss of cytoskeleton-extracellular matrix linkage. *Cell* **80**, 675–679 (1995).
22. Cai, C. *et al.* Membrane repair defects in muscular dystrophy are linked to altered interaction between MG53, caveolin-3, and dysferlin. *J. Biol. Chem.* **284**, 15894–15902 (2009).
23. Bansal, D. & Campbell, K.P. Dysferlin and the plasma membrane repair in muscular dystrophy. *Trends Cell Biol.* **14**, 206–213 (2004).
24. Weisleder, N. *et al.* Recombinant MG53 protein modulates therapeutic cell membrane repair in treatment of muscular dystrophy. *Sci. Transl. Med.* **4**, 139ra185 (2012).
25. Idone, V. *et al.* Repair of injured plasma membrane by rapid Ca^{2+}-dependent endocytosis. *J. Cell Biol.* **180**, 905–914 (2008).
26. Hua, Z. *et al.* v-SNARE composition distinguishes synaptic vesicle pools. *Neuron* **71**, 474–487 (2011).
27. Reddy, A., Caler, E.V. & Andrews, N.W. Plasma membrane repair is mediated by Ca^{2+}-regulated exocytosis of lysosomes. *Cell* **106**, 157–169 (2001).
28. Corrotte, M. *et al.* Caveolae internalization repairs wounded cells and muscle fibers. *Elife* **2**, e00926 (2013).
29. Jimenez, A.J. *et al.* ESCRT machinery is required for plasma membrane repair. *Science* **343**, 1247136 (2014).
30. Demonbreun, A.R. *et al.* Impaired muscle growth and response to insulin-like growth factor 1 in dysferlin-mediated muscular dystrophy. *Hum. Mol. Genet.* **20**, 779–789 (2011).

ONLINE METHODS

Reverse transcription-PCR. Total RNA was extracted from muscle tissues or cultured myoblasts and dissolved in TRIzol (Invitrogen). First-strand cDNA, synthesized with Superscript III RT (Invitrogen), was used for RT-PCR analysis of ML1 expression based on the following intron-spanning primer pair (and L32 control). ML1: forward, 5′-AAACACCCCA GTGTCTCCAG-3′; reverse, 5′-GAATGACACC GACCCAGACT-3′.

L32: forward, 5′-TGGTGAAGCC CAAGATCGTC-3′; reverse, -5′-CTTCTCC GCA CCCTGTTGTC-3′.

Plasmid construction. Generation of the plasmids used in this study (GFP-ML1, mCherry-ML1, CFP-ML1, GCaMP3-ML1, Lamp1-GCaMP3 and Vamp7-pHluorin) was reported previously[13,26].

Western blotting and immunoprecipitation. A standard western blotting protocol was used. Gastrocnemius muscle was lysed with ice-cold radioimmunoprecipitation assay (RIPA) buffer in the presence of 1× protease inhibitor cocktail (Sigma). For each sample, 10–100 μg of total protein was loaded onto 4–12% SDS-polyacrylamide gradient gels (Invitrogen) and transferred to polyvinylidene fluoride (PVDF) membranes. The membranes were blocked for 1 h with 1% (wt/vol) BSA in PBST and incubated with various antibodies to dystrophin (Abcam, 1:1,000), β-dystroglycan (β-DG, 1:100) (Santa Cruz), caveolin-3 (BD Biosciences, 1:5,000), dysferlin (Abcam, 1:5,000), myosin (Iowa Hybridoma Bank, 1:4,000), MG53 (Novus Biologicals, 1:5,000) and Lamp1 (ID4B; Iowa Hybridoma Bank, 1:4,000) in PBST. The blots were detected by using peroxidase-conjugated anti-rabbit, anti-mouse or anti-rat secondary antibody with an enhanced chemiluminescence reagent (Amersham Pharmacia Biotech).

Mouse lines. The generation and characterization of ML1 KO mice (in a B6:129 mixed genetic background) were as described[11,14]. *mdx* mice were ordered from Jackson Laboratories. Fabry's mice[31] were a gift from J. Shayman (University of Michigan). Mice were used under approved animal protocols and the Institutional Animal Care Guidelines at the University of Michigan. WT littermates were used as controls in the mouse experiments. No statistical method was used to predetermine sample size. Mice randomized as to sex were randomly assigned to both control and testing groups, each typically containing 3–5 animals.

Treadmill exercise. Mice were trained to run on an Exer-6M treadmill (Columbus Instruments) with a 15° downhill angle at the speed of 12–20 m/min.

Muscle cell culture. Mouse myoblasts were prepared and cultured as described[32]. Briefly, limb muscles were isolated and dissociated with 1% collagenase and 0.25% trypsin treatment at 37 °C. After preplating on a standard Petri dish (non-tissue culture coated) for 60–90 min to remove fibroblasts, muscle cells were maintained at 37 °C and 5% CO_2 in F10 medium with 20% FBS (Gibco). To induce differentiation, myoblasts were grown to confluence before switching to DMEM containing 5% horse serum. For transient transfections, myoblasts were plated at 70% confluence and transfected using Lipofectamine 2000 reagent (Invitrogen). Live-cell imaging experiments were performed 24–48 h after transfection or at the times indicated for individual experiments.

The myogenic C2C12 mouse myoblast cell line was purchased from the American Type Culture Collection (Manassas). Cells were grown in a humidified environment at 37 °C and 5% CO_2 in DMEM medium supplemented with 20% FBS and penicillin (100 units/ml) and streptomycin (100 μg/ml). C2C12 cell differentiation was induced by switching to DMEM medium containing 5% horse serum.

Fluorescence and time-lapse confocal imaging. Live imaging of C2C12 or primary myoblasts was performed on a heated stage on a spinning disk confocal imaging system, which consisted of an Olympus IX81 inverted microscope, a 60× or 100× objective (Olympus), a CSU-X1 scanner (Yokogawa), an iXon EM-CCD camera (Andor) and MetaMorph Advanced Imaging acquisition software v.7.7.8.0 (Molecular Devices). For immunofluorescence detection, cells or muscle sections were fixed with 4% paraformaldehyde (PFA), permeabilized with 0.03% Triton X-100 and stained with primary antibodies to EEA1 (Abcam, 1:100), Lamp1 (ID4B, 1:100), dystrophin (1:1,000), β-DG (1:10), integrin β1 (1:100) (Iowa Hybridoma Bank) and laminin (Chemicon, 1:200).

Whole-endolysosome electrophysiology. Endolysosomal electrophysiology was performed on isolated endolysosomes with a patch clamp method as described[12,33]. Briefly, cells were treated with 1 μM vacuolin-1 for 2–5 h to increase the size of endosomes and lysosomes. Whole-endolysosome recordings were performed on isolated enlarged endolysosomes. The bath (internal/cytoplasmic) solution contained 140 mM K-gluconate, 4 mM NaCl, 1 mM EGTA, 2 mM Na_2-ATP, 2 mM $MgCl_2$, 0.39 mM $CaCl_2$, 0.2 mM GTP and 10 mM HEPES (pH adjusted with KOH to 7.2; the free $[Ca^{2+}]_i$ was estimated to be ~100 nM on Maxchelator software (http://maxchelator.stanford.edu/)). The pipette (luminal) solution consisted of a 'low-pH Tyrode's solution' with 145 mM NaCl, 5 mM KCl, 2 mM $CaCl_2$, 1 mM $MgCl_2$, 10 mM HEPES, 10 mM MES and 10 mM glucose (pH 4.6). All bath solutions were applied via a perfusion system to achieve a complete solution exchange within a few seconds. Data were collected with an Axopatch 2A patch clamp amplifier, Digidata 1440 and pClamp 10.0 software (Axon Instruments). Currents were digitized at 10 kHz and filtered at 2 kHz. All experiments were conducted at room temperature (21–23 °C), and all recordings were analyzed with pClamp 10.0 and Origin 8.0 (OriginLab).

Whole-cell electrophysiology. Whole-cell recordings were performed as described[13,34]. The pipette solution contained 147 mM Cs, 120 mM methane sulfonate, 4 mM NaCl, 10 mM EGTA, 2 mM Na_2-ATP, 2 mM $MgCl_2$ and 20 mM HEPES (pH 7.2; free $[Ca^{2+}]_i < 10$ nM). The standard extracellular bath solution (modified Tyrode's solution) contained 153 mM NaCl, 5 mM KCl, 2 mM $CaCl_2$, 1 mM $MgCl_2$, 20 mM HEPES and 10 mM glucose (pH 7.4).

GCaMP3 Ca^{2+} imaging. GCaMP3 Ca^{2+} imaging was performed in primary myoblasts or C2C12 cells that were transfected with Lamp1-GCaMP3 or GCaMP3-ML1, which are lysosome-targeted genetically encoded Ca^{2+} sensors[13]. The fluorescence intensity at 488 nm (F_{488}) was recorded with the spinning disk confocal imaging system.

H&E and histochemical staining. H&E staining was performed in 12-μm sections that were prepared from freshly frozen tissues and fixed with 4% PFA. Myosin ATPase staining was performed at pH 4.3; at this pH, type 1 slow-twitch fibers are dark-colored and type 2 fast-twitch fibers are light-colored[35].

Collagen content measurement. The level of hydroxyproline, a major component of collagen[6], was measured using the Hydroxyproline Assay Kit (Sigma).

Sciatic axotomy. Right sciatic nerves of 3-month-old WT mice were exposed, and a 5-mm segment of the nerve was removed surgically. The wound was closed with silk sutures. The gastrocnemius muscle was collected for H&E staining 2 weeks after the axotomy.

Myofiber damage assay. After mice were sacrificed by cervical dislocation, FDB muscles were surgically removed to be digested in a Tyrode's solution containing type I collagenase (2 mg/ml; Sigma) at 37 °C for 60 min. After resuspension in the Tyrode's solution, single FDB fibers were mounted on a glass bottom chamber in Tyrode's or zero Ca^{2+} solution in the presence of 2.5 μM green-colored FM1-43 dye (Molecular Probes). To induce damage to the muscle fibers, a selected region (5 μm × 5 μm) of the plasma membrane was irradiated for 5 s with a two-photon laser (laser power 3700 at wavelength 820 nm) in a Leica Fluoview 300 confocal microscope system. Images were captured at 10-s intervals. For every image taken, the fluorescence intensity at the site of the damage was measured with ImageJ software. Fibers that had defective membrane resealing showed dye accumulation at the injury sites

throughout the time course of the experiment, whereas, for resealed fibers, dye influx stopped typically within 1 min.

Microelectrode penetration damage. C2C12 myoblasts or primary myoblasts were allowed to differentiate into myotubes for 3–5 d before use. Microelectrodes (borosilicate glass capillaries; World Precision Instruments) were connected to a three-axis micromanipulator (MHH-103 Narishige International) to precisely control the penetration of the cell membrane in the presence of 2.5 μM red-colored FM4-64 dye (Molecular Probes). After a microelectrode was gently attached to a myotube, a further displacement of ~2 μm was considered penetration. Images were taken on an Olympus microscope equipped with a QIClick digital CCD Camera (QImaging). Live imaging of myoblasts was performed on a heated stage with the spinning disk confocal imaging system described above. Microelectrodes attached to the three-axis micromanipulator MP-285 (Sutter Instruments) were used to induce penetration. The investigator was blinded to allocation during experiments and outcome assessment.

Evans blue dye uptake. EB dye (1%; 10 ml per kg body weight; Sigma) was injected into the intraperitoneal space of 1-month-old mice 8–16 h before tissue collection. Dissected gastrocnemius muscles were frozen for cryosectioning.

Flow cytometry PI staining. His-tagged SLO (carrying a cysteine deletion that eliminates the need for thiol activation[25]) was provided by R. Tweeten (University of Oklahoma) and purified using Ni-nitrilotriacetic acid (NTA) agarose resin (Qiagen) in a BL21 *E. coli* expression system. The protein concentration was measured using the Bradford assay, and the aliquots of proteins were stored at −80 °C until use. For each experiment, about 2×10^6 cells were trypsinized, washed with Tyrode's solution and incubated with SLO (2–5 μg/ml) for 10 min at 37 °C. Titration of SLO was performed to determine the minimum concentration required for cell permeabilization in 0 Ca^{2+} and the maximum concentration not causing significant cell loss. SLO-treated cells were then stained with 200 μg/ml propidium iodide (PI; Sigma-Aldrich) for 5 min and analyzed by FACS Flow Cytometry (iCyt Synergy; Sony). More than 10,000 cells were used for each condition. Data were analyzed using WinList 3D software (Verity Software House).

Lysosomal enzyme release and activity. Upon SLO treatment for 15 min, the conditioned culture medium was collected for acid phosphatase (AP) and acid sphingomyelinase (aSMase) activity measurement using an AP colorimetric assay kit (Sigma) and an acid sphingomyelinase activity assay Kit (Echelon Biosciences), respectively.

Lamp1 surface staining. C2C12 were incubated with 500–800 ng/ml SLO (a concentration that causes no significant PI staining) at 37 °C for 30 min. Cells were stained with PI, resuspended in 1% BSA with anti-mouse Lamp1 (1D4B) antibody on ice for 45 min, fixed in 2% PFA for 30 min and finally incubated with Alexa-488–conjugated anti-rat secondary antibody (Invitrogen) at room temperature for 1 h. After resuspension in 0.5 ml PBS, cells were analyzed on a FACS Flow Cytometer (MoFlo Astrios, Beckman Coulter). At least 10,000 cells per experiment were analyzed for forward-angle scatter, right-angle scatter and fluorescence intensity.

PHluorin total internal reflection fluorescence imaging. TIRF imaging was performed at 37 °C using a VisiTech Infinity three array-scanning confocal microscope (VisiTech International Ltd.) equipped with a 100× APO TIRF objective oil-immersion (Nikon, NA 1.49). MetaMorph v7.71 image acquisition software was used to process the data.

Electron microcopy analysis. For EM analysis, animals were perfused with 4% PFA and 2.5% glutaraldehyde in PBS. Muscles were surgically removed with intact tendons. Samples were prepared with standard embedding and sectioning procedures.

AAV generation and infection. CAG promoter-driven AAV1/2-GFP-ML1 virus was generated by the Gene Transfer Vector Core of the University of Iowa. Virus injection was performed on one side of the gastrocnemius muscle of 1-month-old ML1 KO or 10-day-old *mdx* mice. The other side of the gastrocnemius muscle was used as the contralateral control. Injected and noninjected contralateral leg muscles were examined after 4 weeks.

Data analysis. Data are presented as the mean ± s.e.m. Statistical comparisons were performed with analysis of variance (ANOVA). A P value <0.05 was considered statistically significant.

31. Bolsover, F.E., Murphy, E., Cipolotti, L., Werring, D.J. & Lachmann, R.H. Cognitive dysfunction and depression in Fabry disease: a systematic review. *J. Inherit. Metab. Dis.* **37**, 177–187 (2014).
32. Springer, M.L., Rando, T.A. & Blau, H.M. Gene delivery to muscle. *Curr. Protoc. Hum. Genet.* **31**, 13.14 (2002).
33. Dong, X.P. *et al.* $PI_{3,5}P_2$ controls membrane traffic by direct activation of mucolipin Ca release channels in the endolysosome. *Nat. Commun.* **1**, 38 (2010).
34. Wang, X. *et al.* TPC proteins are phosphoinositide-activated sodium-selective ion channels in endosomes and lysosomes. *Cell* **151**, 372–383 (2012).
35. Brooke, M.H. & Kaiser, K.K. Muscle fiber types: how many and what kind? *Arch. Neurol.* **23**, 369–379 (1970).

doi:10.1038/nm.3611

Supplementary Figures

An Intracellular Ca^{2+} Channel is Required For Sarcolemma Repair to Prevent Muscular Dystrophy

Xiping Cheng, Xiaoli Zhang, Qiong Gao, Mohammad Ali Samie, Marlene Azar, Wai Lok Tsang, Libing Dong, Nirakar Sahoo, Xinran Li, Yue Zhuo, Abigail G. Garrity, Xiang Wang, Marc Ferrer, James Dowling, Li Xu, Renzhi Han & Haoxing Xu

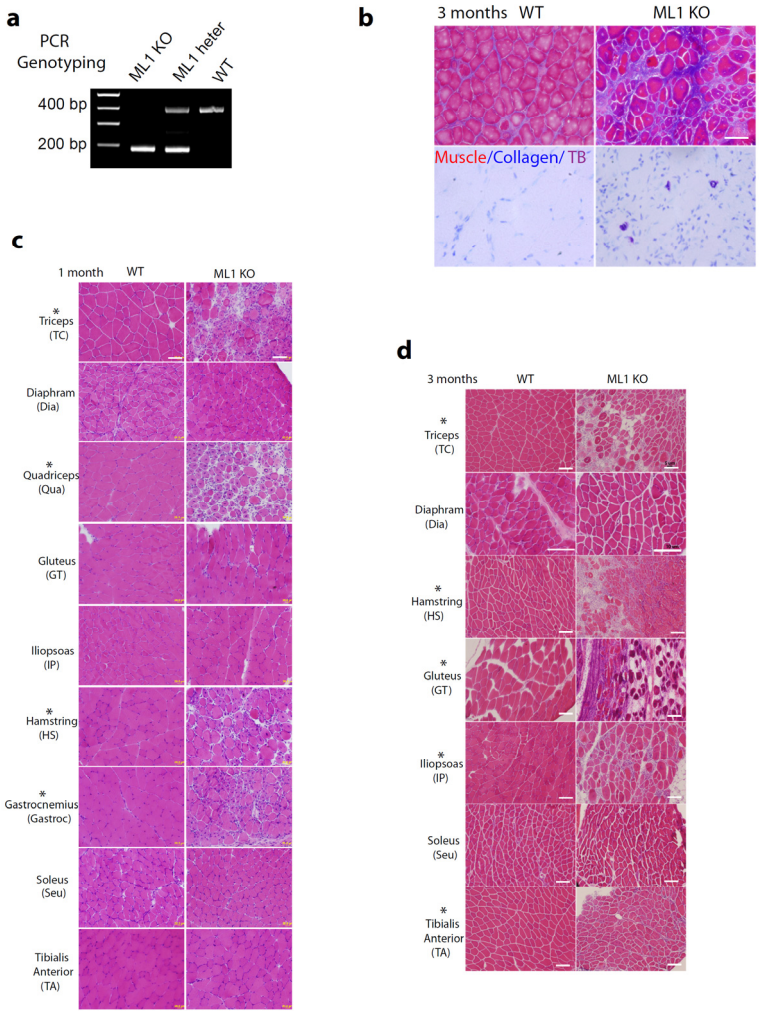

Supplementary Fig. 1 Progressive development of MD in ML1-null mice.
(a) PCR analysis was performed with a primer pair targeting the deleted region (exons 3, 4, and 5) of the *TRPML1* gene[11]. **(b)** Fibrosis was detected by using Gomori's trichrome stain to stain collagen fibers (blue). Infiltration of mast cells was detected with toluidine blue (purple). Scale bar = 40 μm. **(c)** At 1 month of age, only a subset of muscles, including the triceps (TC), quadriceps (Qua), hamstring (HS), and Gastroctrocnemius (Gastroc) muscles, showed fibrosis and centrally nucleated fibers. No significant dystrophy was seen in other skeletal muscles, including the diaphragm (Dia), iliopsoas (IP), soleus (Seu), and tibialis anterior (TA) muscles. Scale bar = 40 μm. **(d)** At 3 months, the IP and TA muscles also exhibited fibrosis and central nucleation. Scale bar = 80 μm.

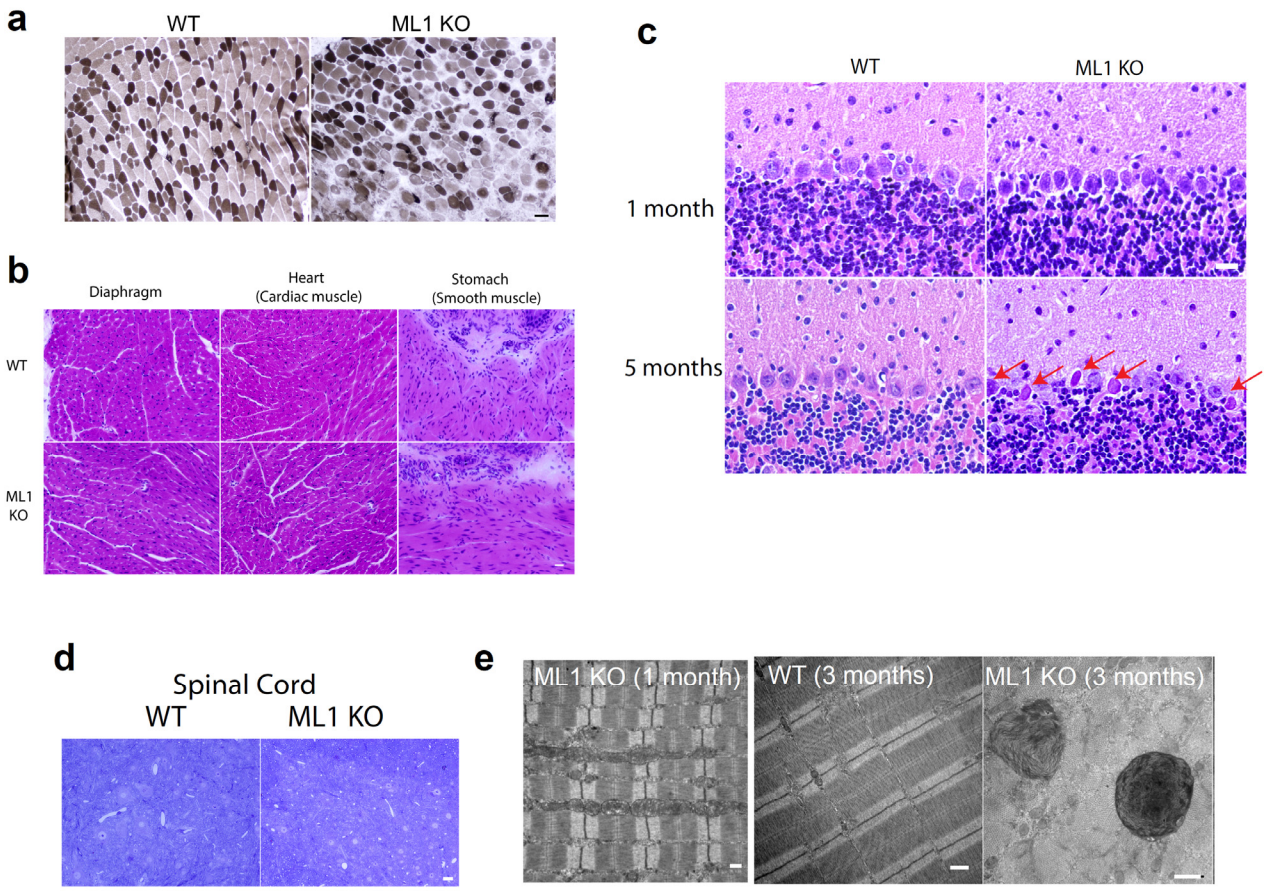

Supplementary Fig. 2 MD of ML1-null mice is not caused by neurodegeneration or chronic lysosomal storage.

(a) Muscular dystrophy in both type I and type II muscle fibers of ML1 KO mice. Myosin ATPase staining (pH of 4.3) was used to distinguish between type 1 (dark) and type 2 (light) muscle fiber types. Scale bar = 50 µm. **(b)** Muscle from 3-month-old WT and ML1 KO mice was stained with H&E. No clear dystrophy was observed in cardiac or smooth muscle from the stomach. Scale bar = 20 µm. **(c)** Dying neurons in H&E-stained mouse brain sections from the cerebellum of 5-month-old ML1 KO mice. Scale bar = 10 µm. **(d)** Toluidine Blue-stained ventral horn sections of WT and ML1 KO. Scale bar = 20 µm. **(e)** Electron microscope analysis on lysosomal storage in muscle fibers from 1 and 3-month-old mice. Scale bar = 500 nm.

Nature Medicine: doi:10.1038/nm.3611

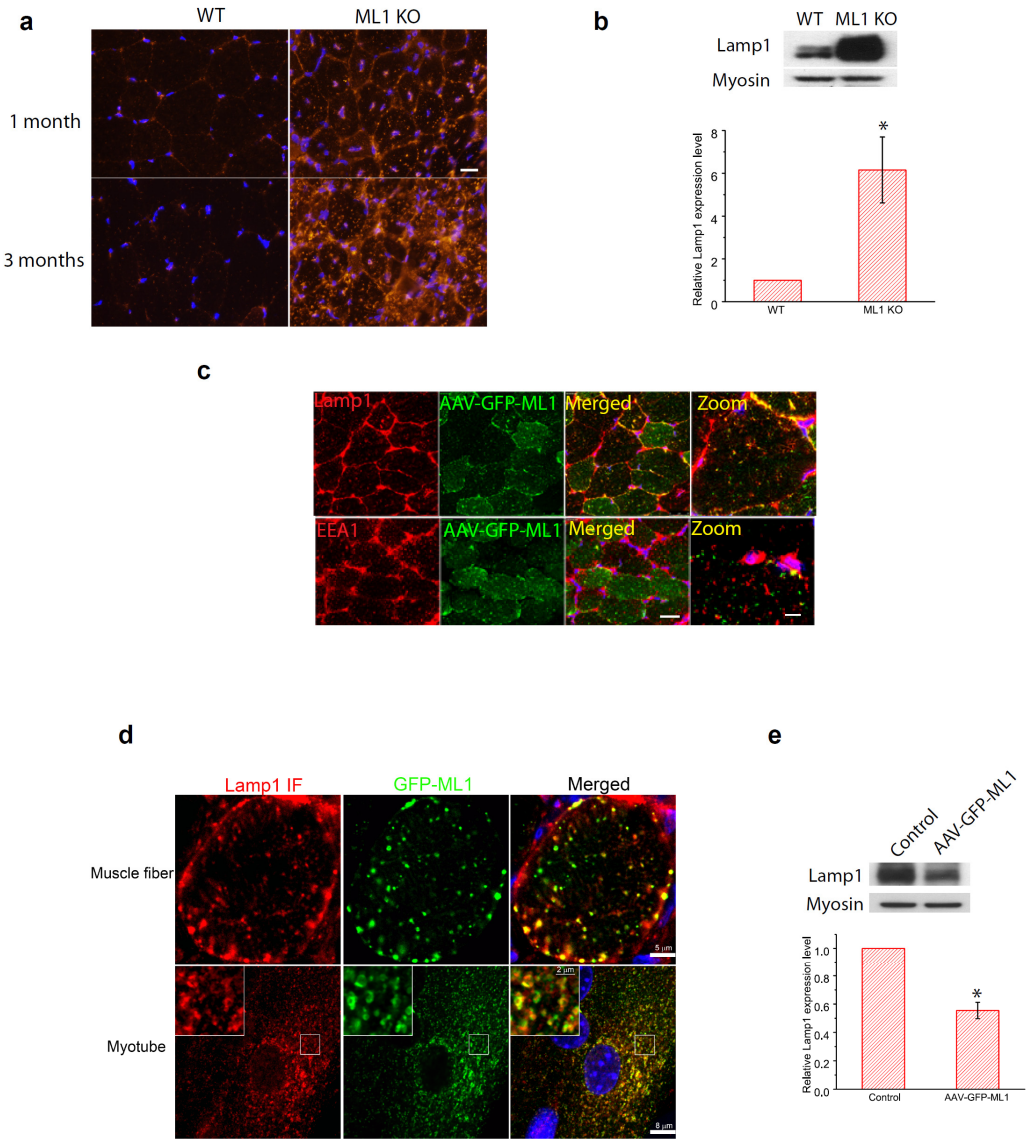

Supplementary Fig. 3 Increased expression of Lamp1 proteins in ML1-null muscle cells is decreased by AAV-GFP-ML1 expression.
(a) Lamp1 immunofluorescence in the skeletal muscle of 1- or 3-month-old ML1 KO skeletal muscle. Scale bar = 10 μm. **(b)** Western blotting showed increased expression of Lamp1 in 1-month-old ML1-null muscle. **(c)** Immunostaining of Lamp1 and EEA1 in AAV-GFP-ML1–infected muscle. Scale bars = 25 μm for the three panels on the left or 5 μm for the zoomed images. **(d)** Immunostaining of Lamp1 in AAV-GFP-ML1-infected myofibers and GFP-ML1 transfected cultured myotubes. Scale bars = 5 μm for the upper panel, 8 μm for the lower panel, and 2 μm for the zoomed image. **(e)** Western blot analysis revealed that the expression level of Lamp1 proteins was decreased when ML1-null muscles were infected with AAV-GFP-ML1. Contralateral uninfected muscle was used as the control. Data are presented as the mean ± s.e.m.

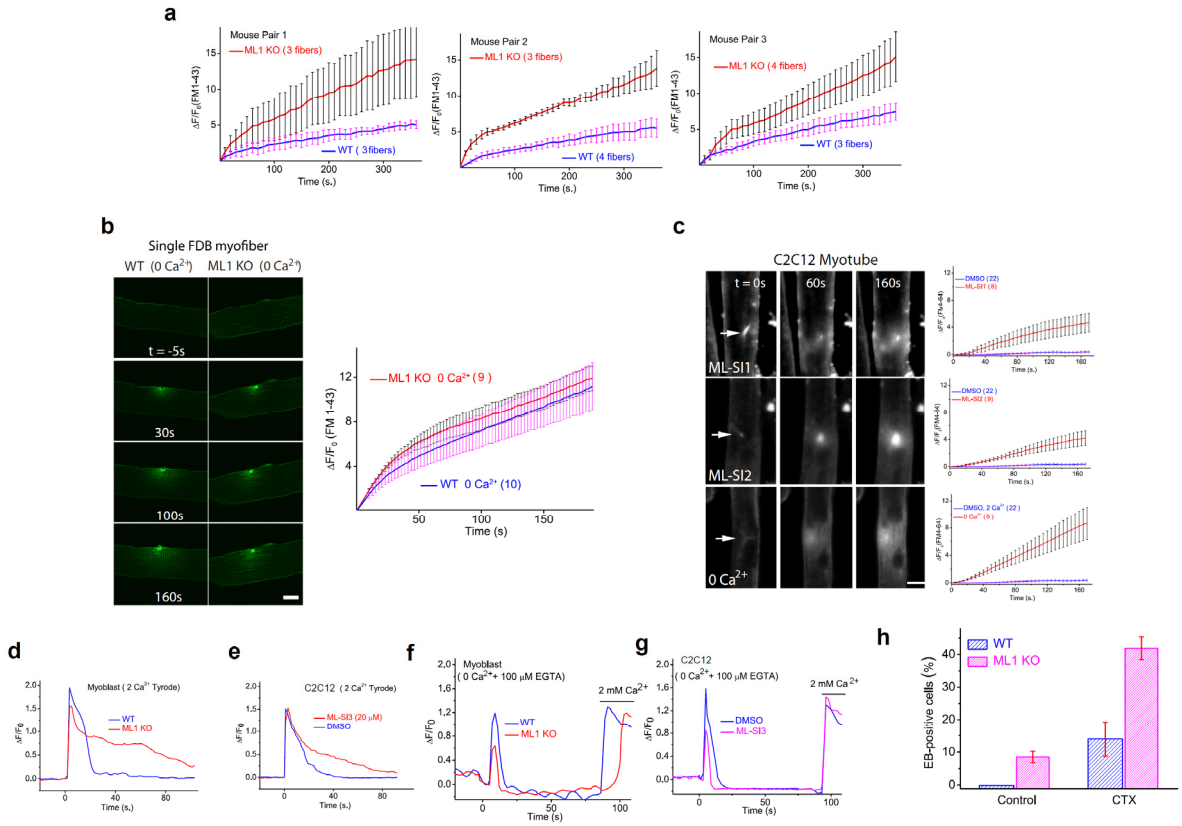

Supplementary Fig. 4. Full capacity of membrane repair in muscle requires ML1 and extracellular Ca^{2+}.

(a) A membrane repair assay performed on single FDB muscle fibers isolated from three pairs of WT and ML1 KO mice. Membrane damage was induced with a two-photon laser at t = 0 s. The time-dependent changes (ΔF) in FM1-43 fluorescence intensity were normalized to the basal fluorescence (F_0) for WT (blue) and ML1 KO (red) fibers. Results from all fibers (n=10 from three pairs of mice) were shown in Fig. 3c. **(b)** Membrane damage was induced in single FDB muscle fibers with a two-photon laser at t = 0 s. In zero extracellular Ca^{2+}, both isolated WT and ML1 KO fibers failed to effectively exclude FM1-43 dye after laser-induced damage. Scale bar = 10 μm. The right panel shows the time-dependent changes (ΔF) in FM1-43 fluorescence intensity normalized to the basal fluorescence (F_0) for WT (blue) and ML1 KO (red) fibers in zero extracellular Ca^{2+}. **(c)** Responses of C2C12-derived myotubes to microelectrode penetration in Tyrode's solution in the presence of DMSO (0.1%; data replotted from Fig. 3e for comparison), ML-SI1 (20 μM), ML-SI2 (20 μM), or in zero extracellular Ca^{2+}. The right panels show the time course of FM4-64 accumulation ($\Delta F/F_0$) at injury sites following microelectrode penetration. Scale bar = 50 μm. **(d)** In the presence of extracellular Ca^{2+}, a rapid and transient increase was seen in Lamp1-GCaMP3 fluorescence at the damage site for WT myoblasts. ML1 KO myoblasts had prolonged Ca^{2+} influx. **(e)** C2C12 myoblasts had prolonged Ca^{2+} influx in the presence of ML-SI3 (20 μM). **(f, g)** In zero extracellular Ca^{2+}, however, reduced intracellular Ca^{2+} release was seen in ML1 KO myoblasts (**f**) and ML-SI3-treated C2C12 myoblasts (**g**). **(h)** EB dye uptake in WT and ML1 KO Gastroc muscles injected with cardiotoxin VII4 (CTX), a cytolytic toxin that disrupts cell membranes in living animals[24]. *n* = 3 animals for each condition. Data are presented as the mean ± s.e.m.

Nature Medicine: doi:10.1038/nm.3611

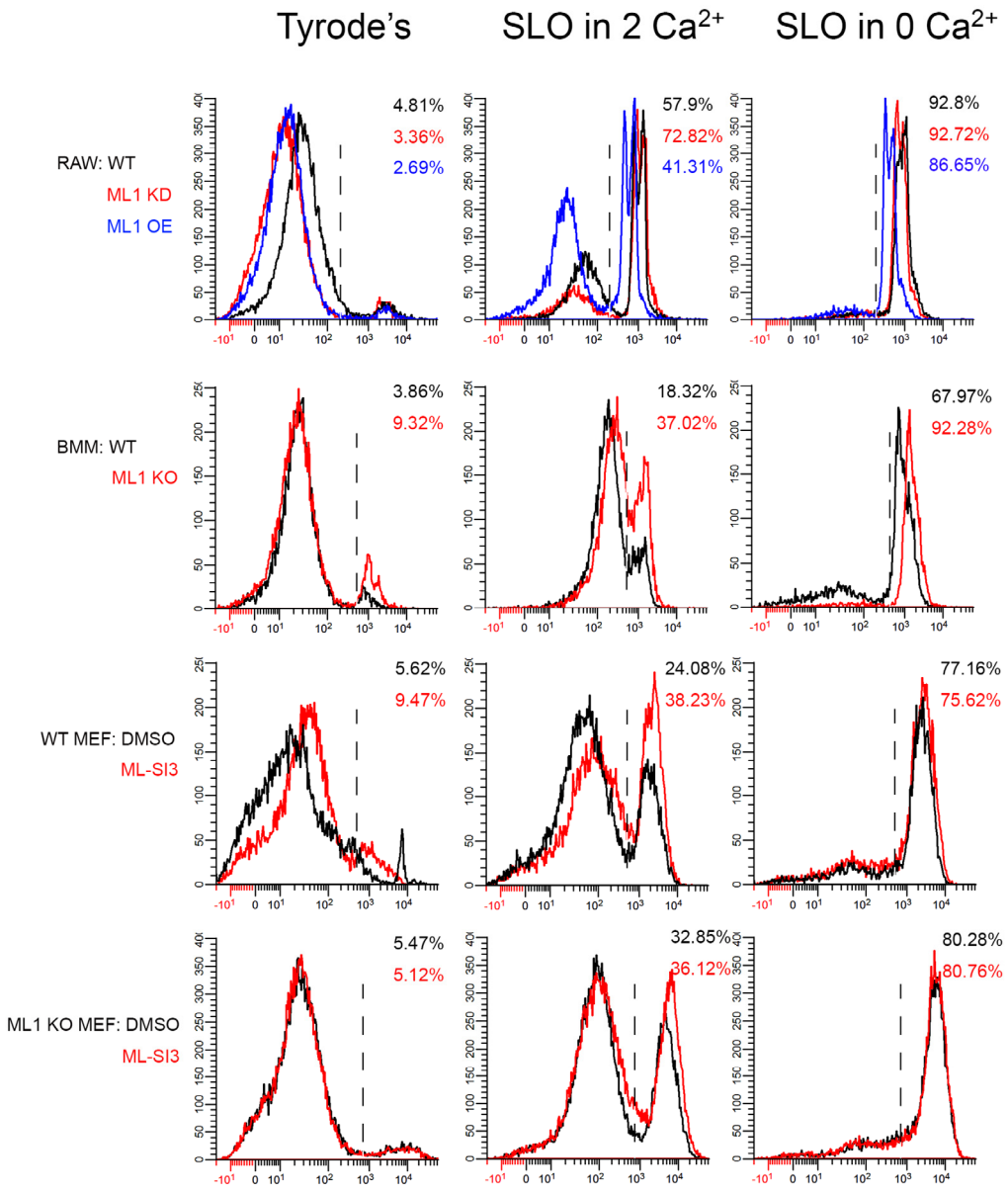

Supplementary Fig. 5. ML1 deficiency or inhibition increases cell's sensitivity to chemical damage.

WT and ML1 KO MEFs, WT and ML1 KO BMMs, and ML1 shRNA knockdown (KD) or overexpressing (O/E) RAW cells were treated with pore-forming toxin streptolysin O (SLO; 2-5 μg/ml), and stained with PI, a marker for membrane damage. FACS quantification of PI staining was performed in cells with or without SLO or external Ca^{2+} (2 mM).

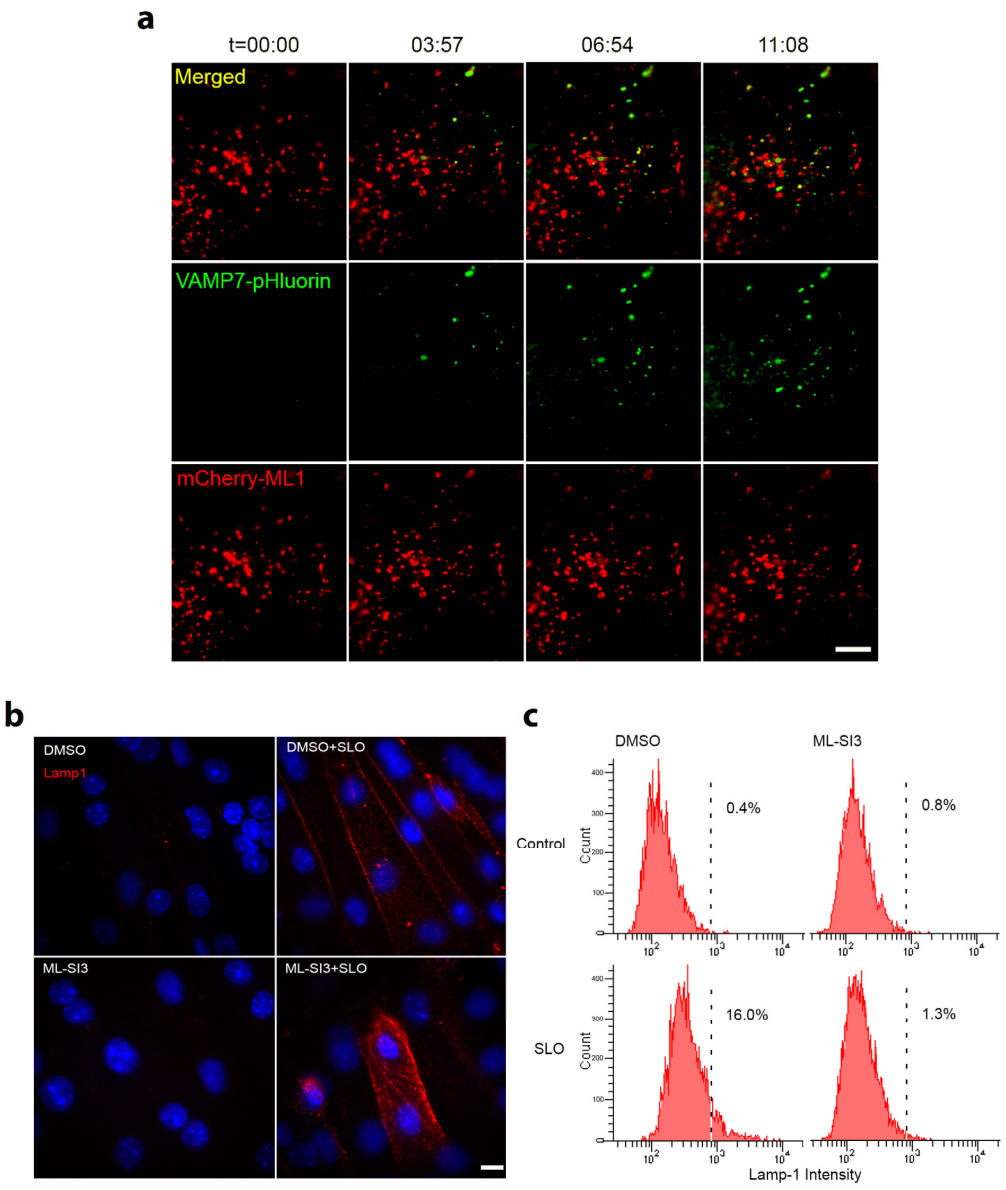

Supplementary Fig. 6 SLO induces lysosomal exocytosis in C2C12 cells.
(a) Fusion of ML1 and VAMP7-pHluorin doubly-positive vesicles with the plasma membrane were visualized by TIRF imaging in COS1 cells upon SLO (0.7 μg/ml) treatment at time zero . Scale bar = 10 μm (related to **Video 1**). **(b)** SLO (0.5-0.8 μg/ml for 30 min) treatment resulted in localization of Lamp1 (red) on the plasma membrane in non-permeabilized C2C12 myotubes. Lamp1 surface expression was detected using an antibody recognizing a luminal epitope (1DB4). ML-SI3 reduced Lamp1 surface staining, but increased cytosolic Lamp1 immunostaining due to membrane disruption and leakage. Scale bar = 10 μm. **(c)** Flow cytometric analysis of SLO-induced Lamp1 surface expression in C2C12 myoblasts. PI-positive cells were eliminated from the analysis.

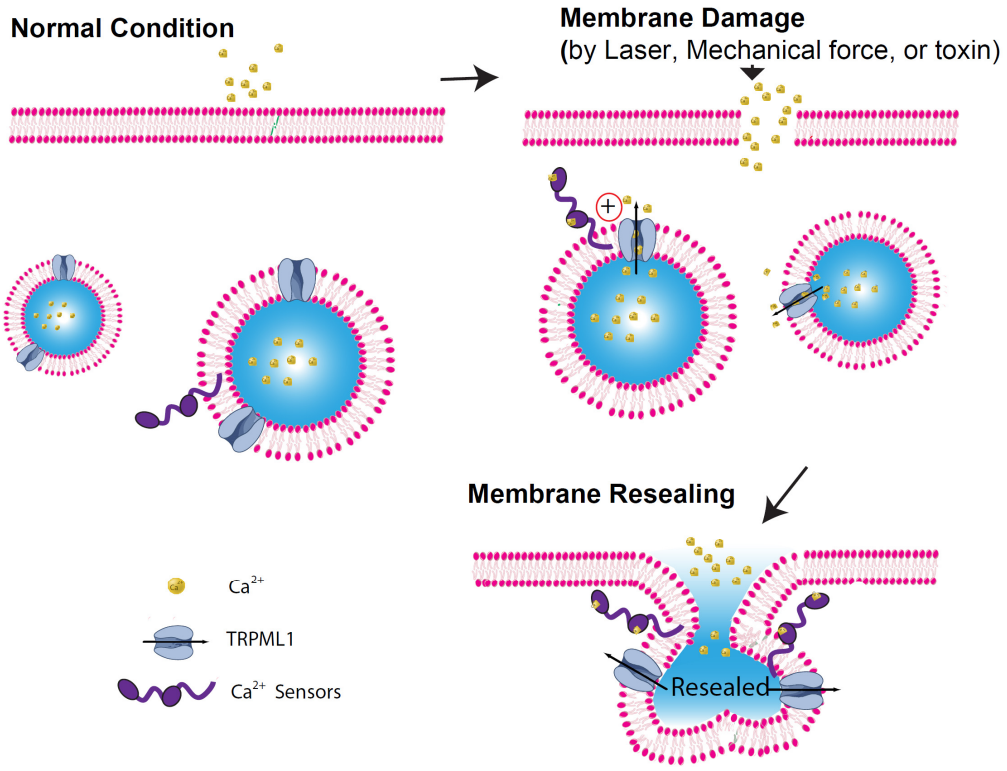

Supplementary Fig. 7. A working model to illustrate the roles of ML1 in membrane repair. Upon membrane damage, ML1 is sensitized or activated to promote lysosomal Ca^{2+} release. Lysosomal Ca^{2+} release, together with Ca^{2+} influx through disrupted membranes, activate multiple Ca^{2+} sensors, such as Syt-VII or dysferlin, to trigger membrane fusion between lysosome and the plasma membrane, resealing the disrupted membranes.

Video 1. SLO treatment induced exocytosis of ML1- and Vamp7-pHluorin-positive vesicles (related to **Supplementary Fig. 6a).** Vesicle fusion with the plasma membrane was visualized using pHluorin-based TIRF imaging upon SLO (0.7 μg/ml) treatment. Scale bar = 10 μm.